The Annals of Applied Statistics
2020, Vol. 14, No. 1, 143–159
https://doi.org/10.1214/19-AOAS1297

SURFACE TEMPERATURE MONITORING IN LIVER PROCUREMENT VIA FUNCTIONAL VARIANCE CHANGE-POINT ANALYSIS

BY ZHENGUO GAO[1], PANG DU[2], RAN JIN[3] AND JOHN L. ROBERTSON[4]

[1]*School of Mathematical Sciences, Shanghai Jiao Tong University, gaozhenguo3@126.com*
[2]*Department of Statistics, Virginia Tech, pangdu@vt.edu*
[3]*Grado Department of Industrial and Systems Engineering, Virginia Tech, jran5@vt.edu*
[4]*School of Biomedical Engineering, Virginia Tech, drbob@vt.edu*

Liver procurement experiments with surface-temperature monitoring motivated Gao et al. (*J. Amer. Statist. Assoc.* **114** (2019) 773–781) to develop a variance change-point detection method under a smoothly-changing mean trend. However, the spotwise change points yielded from their method do not offer immediate information to surgeons since an organ is often transplanted as a whole or in part. We develop a new practical method that can analyze a defined portion of the organ surface at a time. It also provides a novel addition to the developing field of functional data monitoring. Furthermore, numerical challenge emerges for simultaneously modeling the variance functions of 2D locations and the mean function of location and time. The respective sample sizes in the scales of 10,000 and 1,000,000 for modeling these functions make standard spline estimation too costly to be useful. We introduce a multistage subsampling strategy with steps educated by quickly-computable preliminary statistical measures. Extensive simulations show that the new method can efficiently reduce the computational cost and provide reasonable parameter estimates. Application of the new method to our liver surface temperature monitoring data shows its effectiveness in providing accurate status change information for a selected portion of the organ in the experiment.

1. Introduction. According to assessment on May 8, 2018, by the Organ Procurement and Transplantation Network (http://optn.transplant.hrsa.gov/), there are over 110,000 people needing a lifesaving organ transplant, over 70,000 of whom are on the active waiting list. Every 10 minutes someone is added to the national transplant waiting list, and, on average, 22 people die each day while waiting for a transplant. The whole process, from obtaining a donated organ and finding a matching recipient, to the organ being transplanted to the recipient, can often take hours to days. Severely impacting the process, the maximum viability of vital organs, under ideal procurement/preservation conditions, is only four to six hours for lungs and hearts and eight to 12 hours for livers and pancreases. The potential viability of a specific organ can vary from case to case, due to variations in donor health status and quality of procurement. An accurate assessment of an organ's viability status is critical in the process but is difficult to achieve with standard preimplantation organ evaluation methods.

The current practice of organ viability assessment is mainly through two approaches: visual inspection and biopsy (Keeffe (2001), Vazquez-Martul and Papadimitriou (2004)). Visual inspection undoubtedly suffers from human observer subjectivity and experience; in many cases the appearance of a viable organ may be indistinguishable from an unviable one. The use of biopsy and histologic analysis is more accurate but often destroys the portion of organ where the biopsy sample is collected (Lan, Jin and Robertson (2015), Rothuizen and Twedt (2009)). Additionally, the very small volume of a biopsy specimen (<0.5 cm^3)

Received November 2018; revised September 2019.
Key words and phrases. Functional variance change point, thin-plate splines; subsampling, functional data, liver procurement.

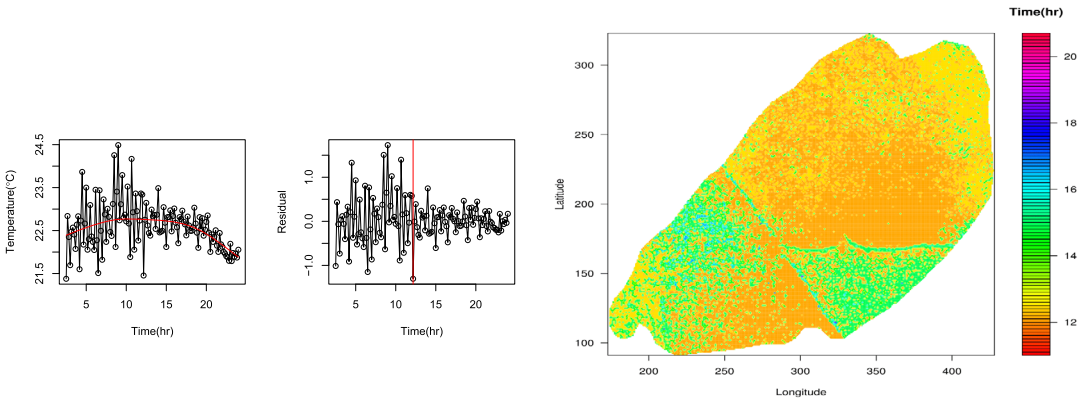

FIG. 1. *Data collected from isolated and machine-perfused porcine liver specimens. Left and middle*: *The raw temperature profile and detrended temperature profile, with the fitted mean function and estimated variance change point imposed, at a random spot of the liver surface. The horizontal axis labels in both panels represent* 24 *hours. Right*: *The heat map of estimated spotwise variance change points of temperatures on a lobe of liver in the procurement experiment.*

may not accurately represent the histomorphology of the entire organ. A research team at Virginia Tech, composed of clinical scientists and engineers, is devising methods for noninvasive monitoring of the viability status of isolated and machine-perfused organs (Bhonsle et al. (2016), Gao et al. (2019), Lan et al. (2018), O'Brien et al. (2017)). We have employed a noninvasive thermal imaging system that can accurately measure the surface temperatures of an organ during machine perfusion. The temperatures are taken at a dense mesh of grid points covering the whole surface of the organ. As an example, the left and center panels in Figure 1 show the raw and detrended temperature profiles of a random spot on the surface of an isolated and machine-perfused liver. Our preliminary analysis of data collected from experiments with porcine livers reveals a close relationship between the histomorphologic quality and surface temperatures of the organ. Such a strong correlation of surface temperature of organs to their viability is also founded in the literature (Karpelowsky (2014), Kochan et al. (2015), Vidal et al. (2014)). In particular, the temperature profiles show a high variation when the corresponding part of the organ is viable, and the variation drops sharply when the viability of that part of organ deteriorates. Thus, identifying the change point of the temperature variation essentially determines the viability breakdown point of the liver. Therefore, our goal is to develop an analytic method for estimating this variation change point beyond which the organ would be considered nonviable.

Existing change point detection methods mostly assume a *sudden* change in a few parameters of the data distribution or the distribution itself as a whole entity. However, the surface temperature data in our experiments have a smoothly changing mean function and, thus, a constantly changing distribution. Blindly applying these methods would result in erroneous change-point estimates. In a recent product of the project, Gao et al. (2019) focused on *spotwise* data analysis and developed a new variance change-point detection method that allows the existence of a smoothly changing mean function. They designed an iterative procedure to simultaneously estimate the mean function, variances and variance change point. Their asymptotic theory included the asymptotic null distribution of the test statistic on variance change point as well as the convergence rates of all the parameter estimates. The final product from the application of the method was a heat map of change points on the surface of the liver as shown in the right panel of Figure 1. In clinical practice a liver is always transplanted as a whole or as a segment of the whole organ. In either case the surgeon needs to know the viability of the whole organ or the selected portion of it. Although the heat map provides

some useful *spotwise* viability information of the liver, it does not necessarily provide immediate information for the surgeon to make a decision. An ideal statistical procedure should provide the viability status of a portion of or the whole organ. This would require extending Gao et al. (2019) to estimating the change point of a variance function on a 2D surface in the presence of a smoothly changing mean function on a 3D space of time and location.

However, such an extension is not trivial. As discussed in the review paper by Woodall et al. (2004), monitoring of nonlinear profiles (functions) is a much harder problem than monitoring a single or multiple scalar parameters. The literature on monitoring functional parameters is much sparser than that on monitoring scalar parameters. Some examples are described below besides those earlier attempts reviewed in Woodall et al. (2004). Febrero, Galeano and González-Manteiga (2008) considered a functional depth approach to outlier detection of functional data where the depth threshold for outliers was obtained through a smooth bootstrap procedure. Zou, Tsung and Wang (2008) proposed the first formal nonlinear profile monitoring procedure through local linear smoothing, taking advantage of the generalized likelihood ratio test developed in Fan, Zhang and Zhang (2001). Qiu, Zou and Wang (2010) extended their approach to monitoring correlated nonlinear profiles through nonparametric mixed-effects local linear models. Berkes et al. (2009) and Yu, Zou and Wang (2012) considered a functional principal component approach to change point detection in the mean of functional data. The common focus of the existing work on monitoring functional parameter is the mean function. As far as we know, there is no work studying change point in a variance function, not even to mention the additional complication imposed by the presence of a smoothly changing mean function.

In addition to the necessary methodological innovation, we also need to be creative in the computational aspect for the multidimensional scenario. Naturally, the variance functions are modeled by thin-plate splines on a 2D space and the mean function by the tensor product of thin-plate splines (location) and cubic splines (time). The surface shown in Figure 1 consists of over 30,000 grid points. Even a small portion of the organ contains thousands to tens of thousand of locations. At each location there are over 100 time points. Therefore, the total sample size can easily reach the magnitude of millions. This is a daunting task for multivariate spline smoothing even with the availability of modern computing power. Kim and Gu (2004) proposed a reduction of the number of knots for smoothing splines that can cut down the computational cost from the cubic order of sample size to a sub-quadratic order. Despite its success for medium-sized data, this approach does not offer a cure to the computational problem when the sample size goes beyond thousands, since the enormous data matrix would be too computationally challenging for all the matrix operations involved. We need an alternative approach for large sample data.

The existing work on nonparametric smoothing with large data sets mostly uses the idea of divide and conquer (D&C). The D&C approach consists of three steps: divide the whole data into subsets, fit the model to each subset and recombine estimates from all the subsets into an overall estimate. Examples include Zhang, Duchi and Wainwright (2015) for kernel ridge regression and Shang and Cheng (2017) and Xu and Wang (2018) for univariate smoothing splines. However, the extension of D&C to modeling of our temperature monitoring experiment may have some other issues. On one hand, a simple random partition of the data does not take full advantage of the dense and regular sampling feature of our data. On the other hand, a sequential partition similar to Xu and Wang (2018) is much harder to implement for a 2D or 3D space. In addition, no matter how the data are partitioned, the ensuing recombining step can be cumbersome since we must estimate a 3D mean function and two 2D variance functions as well as test on the existence of a variance function change point. Therefore, we adopt the subsampling approach in this work which has been well-received in the past decade due to the need of efficient statistical analysis methods to handle massive data sets. For example, Rokhlin and Tygert (2008), Drineas et al. (2011), Ma, Mahoney and Yu (2015), Ma and

Sun (2015) and Wang, Yang and Stufken (2019) designed various subsampling algorithms for linear regression with massive data. Jin, Chang and Shi (2011) studied subsampling under the Gaussian process models for spatial correlated data. Fithian and Hastie (2014) and Wang, Zhu and Ma (2018) studied subsampling for logistic regression on massive data.

The main computational difficulty in extending the method of Gao et al. (2019) to the multivariate case is the exponential increase in the sample size. To overcome this, we introduce a three-stage subsampling strategy here. The first stage is a blockwise subsampling of locations, the second stage a reduction in time points and the third stage a probability-weighted sub-subsampling of locations. The latter two stages take advantage of a preliminary spotwise analysis applying Gao et al. (2019) to the stage-one subsample. After the three-stage subsampling, we then extend the method of Gao et al. (2019) to the multivariate case to analyze the final subsample. Our simulations demonstrate the computational efficiency of the proposed method while maintaining a good estimation performance. The application of our method to the liver procurement experiment yield direct viability information about any selected region of the organ.

In summary, our method has the following distinguishing features: (1) it is uniquely qualified to address the scientific goal for our liver procurement experiment, identifying the viability breakdown point of the liver; (2) it is an innovative addition to the developing literature on change-point analysis for functional data given its unique focus on change in a sequence of 2D variance functions; (3) it provides a nontrivial extension of the existing subsampling approach to a rather complex problem setting.

The rest of the paper is organized as follows. We introduce our method in Section 2. In Section 3 we present all the simulations. We analyze the liver procurement data in Section 4. Discussion in Section 5 concludes the paper.

2. Method.

2.1. *Notation and model.* In the following we shall use the superscript ^{0} to represent the original data and the subscript $_0$ the underlying truth. Suppose that surface temperature measurements y_{ij}^0 are independent observations generated from the following model:

$$y_{ij}^0 = f_0(i/N, z_j^0) + \epsilon_{ij}, \quad i = 1, \ldots, N, j = 1, \ldots, M, \tag{2.1}$$

where M is the number of locations, N is the number of sampling time points, $z_j^0 = (z_{1j}^0, z_{2j}^0) \in \mathbb{R}^2$ is the jth location (latitude and longitude), $f_0(t, z)$ is an unknown smooth mean function of time t and location z and the random errors $\epsilon_{ij} \sim N(0, \sigma_i^2(z_j^0))$ where $\sigma_i^2(\cdot)$ is the variance function of location at the ith time point. To identify the viability breakdown point, we are interested in testing the hypothesis

$$\mathbf{H}_0 : \sigma_1^2(z) = \cdots = \sigma_N^2(z) \quad \text{vs.}$$

$$\mathbf{H}_1 : \sigma_1^2(z) = \cdots = \sigma_{\tau_0}^2(z) \neq \sigma_{\tau_0+1}^2(z) = \cdots = \sigma_N^2(z) \quad \text{for some } \tau_0.$$

Note that $\mathbf{H}_0$ is equivalent to $\tau_0 = N$. Therefore, without loss of generality, we shall assume that $\sigma_i^2(z) = \sigma_0^2(z)$ when $i \leq \tau_0$, and $\sigma_i^2(z) = \delta_0^2(z)$ when $i > \tau_0$, where both $\sigma_0^2(\cdot)$ and $\delta_0^2(\cdot)$ are unknown smooth-positive functions. Next, we present the computational algorithm for our method and leave the details of each step to subsequent subsections.

ALGORITHM.

1. Three-stage subsampling (see Section 2.3):
   (a) Divide the region of interest into m_1 equal-sized small blocks, and randomly select one location from each block to form the initial subsample Z_1 of m_1 locations.

(b) Perform the spotwise analysis of Gao et al. (2019) at the locations in Z_1, calculate the average of all the spotwise variance change points and compute a time window $T = \{t_1, \ldots, t_n\}$ of size n centered at the average change point.
(c) Calculate a probability weight for each location in Z_1 based on statistics from the spotwise analysis. Sample m locations from Z_1 with these probability weights to obtain the final location subsample $Z = \{z_1, \ldots, z_m\}$.

2. Iterative estimation of mean function and variance change point on $T \times Z$:
(a) Initialize $\widehat{f}^{(0)}$ with the mean-function estimate assuming constant variance.
(b) Iterate on the following two steps until convergence. At the ιth iteration:
i. Given the mean estimate $\widehat{f}^{(\iota-1)}$, we first use the testing procedure in Section 2.4 to find an estimate $\widehat{\tau}^{(\iota)}$ for τ_0. Then, at each location z_j in Z, we compute the maximum likelihood estimates $[\widehat{\sigma}_j^2]^{(\iota)}$ and $[\widehat{\delta}_j^2]^{(\iota)}$ using the respective subsequences of residuals, $\{y_{ij} - \widehat{f}^{(\iota-1)}(t_i, z_j) : i = 1, \ldots, \widehat{\tau}^{(\iota)}, \}$ and $\{y_{ij} - \widehat{f}^{(\iota-1)}(t_i, z_j) : i = \widehat{\tau}^{(\iota)} + 1, \ldots, n\}$.
ii. Now, given the variance component estimates $\widehat{\tau}^{(\iota)}$, $[\widehat{\sigma}_j^2]^{(\iota)}$ and $[\widehat{\delta}_j^2]^{(\iota)}$, we update the mean estimate by the minimizer of (2.2) where the covariance matrix Σ is updated with the current variance component estimates.

3. Repeat Step 1 subsampling and Step 2 estimation K times. Denote the K sets of mean function and change-point estimates as $\{(\widehat{f}_1, \widehat{\tau}_1), \ldots, (\widehat{f}_K, \widehat{\tau}_K)\}$. Then, our final mean and change-point estimates are, respectively, $\widehat{f} = \sum_{k=1}^{K} \widehat{f}_k/K$ and $\widehat{\tau} = \sum_{k=1}^{K} \widehat{\tau}_k/K$.

4. Use the whole data and the mean estimate $\widehat{f}$ to compute the residuals $\{\hat{\epsilon}_{ij} = y_{ij}^0 - \widehat{f}(i/N, z_j^0), i = 1, \ldots, N; j = 1, \ldots, M\}$. Use thin-plate splines to smooth the squared residuals $\{\hat{\epsilon}_{ij}^2, i = 1, \ldots, \widehat{\tau}; j = 1, \ldots, M\}$ and $\{\hat{\epsilon}_{ij}^2, i = \widehat{\tau} + 1, \ldots, N; j = 1, \ldots, M\}$, respectively, to obtain the final variance-function estimates $\widehat{\sigma}^2(z)$ and $\widehat{\delta}^2(z)$.

In the algorithm, the final estimates for the variance functions σ_0^2 and δ_0^2 use thin-plate splines. All the intermediate and final estimates of the mean function f_0 use tensor product of cubic and thin-plate splines. The knots selection procedure suggested in Kim and Gu (2004) is used in all these estimations. Therefore, if sufficient smoothness ($p = 2$ in Kim and Gu (2004)) is assumed for the true functions, the computational costs for each variance function estimation and each mean function estimation are, respectively, of (approximate) orders $O(m^{9/5})$ and $O(m^{9/5}n^{9/5})$. Had the original data been used for these estimations, these costs would be in terms of M and N instead. The convergence criterion used in Step 2(b) is the maximum absolute difference between the residuals of the current iteration versus the previous iteration. This step usually converges in a few iterations in our numerical experiments.

2.2. *Smoothing splines estimation.* All the function parameters will be estimated by smoothing splines under the setting of nonparametric regression. Therefore, we will give a short review of smoothing splines regression in this section. We start with a generic setting. Let (Y_i, x_i) be independent observations generated from the regression model $Y_i = \eta_0(x_i) + \epsilon_i$, $i = 1, \ldots, I$, where Y_i is a continuous response variable, $x_i \in \mathcal{X}$ is a generic predictor that can be univariate or multivariate, η_0 is the unknown smooth function of interest and ϵ_i are independently distributed random errors with mean 0 and variance σ_i^2. Assume η_0 belongs to a reproducing kernel Hilbert space $\mathcal{H} = \{\eta | \eta : \mathcal{X} \to \mathbb{R}, J(\eta) < \infty\}$, where J is seminorm on $\mathcal{H}$. Some examples of J and $\mathcal{H}$ to be used in the paper will be given later. Let $\Sigma = \text{diag}(\sigma_1^2, \ldots, \sigma_I^2)$. Given Σ, the smoothing splines estimate of η is the minimizer of the penalized weighted least squares

$$\frac{1}{I}(\mathbf{Y} - \boldsymbol{\eta})^T \Sigma^{-1} (\mathbf{Y} - \boldsymbol{\eta}) + \lambda J(\eta) \tag{2.2}$$

in $\mathcal{H}$, where $\mathbf{Y} = (Y_1, \ldots, Y_I)^T$, $\boldsymbol{\eta} = (\eta(x_1), \ldots, \eta(x_I))^T$, $J(\eta)$ acts as a roughness penalty and $\lambda > 0$ is the smoothing parameter balancing the trade-off between the goodness-of-fit and smoothness of the mean-function estimate. When the random errors have a common variance, the matrix Σ^{-1} can be dropped from (2.2) since the common variance can be absorbed into λ. Then, (2.2) reduces to the penalized least squares

$$\frac{1}{I}(\mathbf{Y} - \boldsymbol{\eta})^T(\mathbf{Y} - \boldsymbol{\eta}) + \lambda J(\eta). \tag{2.3}$$

A reproducing kernel Hilbert space (RKHS) is a Hilbert space $\mathcal{H}$ where the evaluation functional $[x] : \mathcal{H} \to \mathbb{R}$, $\eta \mapsto \eta(x)$ is continuous for every $x \in \mathcal{X}$. By the Riesz Representation Theorem, for each $x \in \mathcal{X}$ there exists a unique function $R_x \in \mathcal{H}$ with the reproducing property $\langle R_x, \eta\rangle = [x](\eta) = \eta(x)$, where $\langle \cdot, \cdot \rangle$ is the inner product on $\mathcal{H}$. Now, the reproducing kernel R of $\mathcal{H}$ is defined as a function $R : \mathcal{X} \times \mathcal{X} \to \mathbb{R}$ such that $R(x, u) = \langle R_x, R_u\rangle$. One can show that each RKHS is uniquely associated with a reproducing kernel and vice versa. Note that the penalty functional J in (2.2) is a squared seminorm on $\mathcal{H}$. The null space of J, namely $\mathcal{N}_J = \{f : J(f) = 0\}$, induces a direct sum decomposition $\mathcal{H} = \mathcal{N}_J \oplus \mathcal{H}_J$, where $\mathcal{H}_J$ is the complement of $\mathcal{N}_J$ in $\mathcal{H}$. This then yields a decomposition of the reproducing kernel $R = R_0 + R_J$, where R_0 and R_J are, respectively, the reproducing kernels on the subspaces $\mathcal{N}_J$ and $\mathcal{H}_J$. See, for example, Gu ((2013), Chapter 2) for more details on RKHSs.

The RKHS $\mathcal{H}$ is of infinite dimensions, so a direct optimization of (2.2) on $\mathcal{H}$ seems infeasible. However, since the weighted least squares part in (2.2) depends on η only through its evaluations at the observation points $x_i, i = 1, \ldots, I$, the representer theorem (Wahba (1990)) guarantees that the exact minimizer of (2.2) actually resides in a finite dimensional subspace of $\mathcal{H}$, namely, $\mathcal{N}_J \oplus \operatorname{span}\{R_J(x_1, \cdot), \ldots, R_J(x_I, \cdot)\}$. Let $\phi_l, l = 1, \ldots, a$ be the basis functions of N_J and $\xi_j = R_J(x_j, \cdot)$, $j = 1, \ldots, I$. Write $f = \boldsymbol{\phi}^T\mathbf{d} + \boldsymbol{\xi}^T\mathbf{c}$, where $\mathbf{c}$ and $\mathbf{d}$ are the corresponding coefficient vectors. Also, note that $J(\eta)$ can be written as a quadratic form $J(f) = \mathbf{c}^T Q\mathbf{c}$, where Q is the $I \times I$ matrix with the (i, j)th entry equal to $R_J(x_i, x_j)$. So for a fixed λ, the objective function (2.2) is reduced to a quadratic function of the coefficient vectors $\mathbf{c}$ and $\mathbf{d}$. Its minimizer can be obtained analytically. To select the smoothing parameter λ, an outer loop for minimizing the generalized cross-validation (GCV) score is sufficient for the job; see Gu (2013), Section 3.2.

We now introduce three examples of smoothing splines to illustrate these concepts. The cubic smoothing splines (Example 2.1) will be used for estimating mean functions of time only in the preliminary spotwise analysis. The thin-plate splines (Example 2.2) will be used for computing the final estimates of the variance functions of location. The tensor product splines of cubic and thin-plate splines (Example 2.3) will be used for estimating the mean functions of time and location.

EXAMPLE 2.1 (Cubic-smoothing splines). Suppose $x = t$ is a variable of time and, without loss of generality, assume $\mathcal{X} = \mathcal{T} = [0, 1]$. A choice of $J(f)$ is $\int_0^1 (f'')^2\,dt$ which yields the popular cubic splines. If the inner product in $\mathcal{N}_J$ is $(\int_0^1 f\,dt)(\int_0^1 g\,dt) + (\int_0^1 f'\,dt)(\int_0^1 g'\,dt)$, then $\mathcal{H}_J = \mathcal{H} \ominus \mathcal{N}_J = \{f : \int_0^1 f\,dt = \int_0^1 f'\,dt = 0, J(f) < \infty\}$ and the reproducing kernel $R_J(s, t) = k_2(s)k_2(t) - k_4(|s - t|)$, where $k_\nu(t) = B_\nu(t)/\nu!$ are scaled Bernoulli polynomials for $t \in [0, 1]$. The null space $\mathcal{N}_J$ has a basis $\{1, k_1(t)\}$ of two functions where $k_1(t) = t - 0.5$ for $t \in [0, 1]$. See Gu (2013), Section 2.3.3.

EXAMPLE 2.2 (Thin-plate splines). Suppose $x = z = (z_1, z_2)$ is a variable of 2D location and $\mathcal{X} = \mathcal{Z} = (-\infty, \infty)^2$. For the order 2 thin-plate splines, $J(f) = \iint (\ddot{f}_{11}^2 + 2\ddot{f}_{12}^2 + \ddot{f}_{22}^2)\,dz_1\,dz_2$, where $\ddot{f}_{\langle ij\rangle} = \partial^2 f/\partial z_i \partial z_j$. The null space of J is $\mathcal{N}_J = \operatorname{span}\{1, z_1, z_2\}$, and its

complement space is $\mathcal{H}_J = \mathcal{H} \ominus \mathcal{N}_J$. By Theorem 4 of Duchon (1977), the minimizer η_λ of (2.3) has the expression

$$\eta_\lambda(z) = d_1 + d_2 z_1 + d_3 z_2 + \sum_{i=1}^{n} c_i \|z_i - z\|^2 \log \|z_i - z\|,$$

where d_j and c_i are coefficients and $\|\cdot\|$ is the Euclidean norm. See Gu (2013), Section 4.3.

EXAMPLE 2.3 (Tensor product splines). Suppose $x = (t, z)$ is a multivariate variable of time t and 2D location z and $\mathcal{X} = \mathcal{T} \times \mathcal{Z} = [0, 1] \times (-\infty, \infty)^2$. Example 2.1 gives a decomposition of the RKHS $\mathcal{H}_{\langle t \rangle}$ on the time domain

$$\begin{aligned}\mathcal{H}_{\langle t \rangle} &= \left\{ f : \int_0^1 (f'')^2 \, dt < \infty \right\} = \mathcal{H}_{00\langle t \rangle} \oplus \mathcal{H}_{01\langle t \rangle} \oplus \mathcal{H}_{1\langle t \rangle} \\ &= \operatorname{span}\{1\} \oplus \operatorname{span}\{k_1(t)\} \oplus \left\{ f : \int_0^1 f \, dt = \int_0^1 \dot{f} \, dt = 0, \int_0^1 (f'')^2 \, dt < \infty \right\}.\end{aligned}$$

Example 2.2 gives the decomposition of $\mathcal{H}_{\langle z \rangle} = \mathcal{H}_{00\langle z \rangle} \oplus \mathcal{H}_{01\langle z \rangle} \oplus \mathcal{H}_{1\langle z \rangle} = \operatorname{span}\{1\} \oplus \operatorname{span}\{z_1, z_2\} \oplus \mathcal{H}_{1\langle z \rangle}$, where $\mathcal{H}_{1\langle z \rangle} = \mathcal{H}_{\langle z \rangle} \ominus (\mathcal{H}_{00\langle z \rangle} \oplus \mathcal{H}_{01\langle z \rangle})$.

Taking tensor product of $\mathcal{H}_{\langle t \rangle}$ and $\mathcal{H}_{\langle z \rangle}$, one obtains six tensor sum terms $\mathcal{H}_{\nu,\mu} = \mathcal{H}_{\nu\langle t \rangle} \otimes \mathcal{H}_{\mu\langle z \rangle}$ on $\mathcal{T} \times \mathcal{Z}$, $\nu = 00, 01, 1$ and $\mu = 00, 01, 1$. The two subspaces with $\nu = 00, 01$ and $\mu = 00, 01$ can be lumped together as $\mathcal{N}_J$. The other four subspaces can be put together as $\mathcal{H}_J$. For interpretation, the six subspaces readily define an ANOVA decomposition

$$f(t, z) = f_\varnothing + f_t(t) + f_z(z) + f_{tz}(t, z)$$

for functions on $\mathcal{T} \times \mathcal{Z}$, with $f_\varnothing \in \mathcal{H}_{00\langle t \rangle} \otimes \mathcal{H}_{00\langle z \rangle}$ being the constant term, $f_t \in \{\mathcal{H}_{01\langle t \rangle} \oplus \mathcal{H}_{1\langle t \rangle}\} \otimes \mathcal{H}_{00\langle z \rangle}$ the time main effect, $f_z \in \mathcal{H}_{00\langle t \rangle} \otimes \{\mathcal{H}_{01\langle z \rangle} \oplus \mathcal{H}_{1\langle z \rangle}\}$ the location main effect and $f_{tz} \in \{\mathcal{H}_{01\langle t \rangle} \oplus \mathcal{H}_{1\langle t \rangle}\} \otimes \{H_{01\langle z \rangle} + H_{1\langle z \rangle}\}$ the interaction. In this paper we only consider the additive model for fitting the mean function, that is, the model with $f_{tz} = 0$.

2.3. *Three-stage subsampling*. To take full advantage of the dense nature of our data in both space and time, we first use a blockwise random sampling to select the locations. We divide the region of interest into m_1 small blocks, all equal-sized rectangles except for the corner blocks. Then, one location is randomly selected from each block to form the initial subsample Z_1 of m_1 locations. Note that a spotwise preliminary analysis by the method of Gao et al. (2019) needs to be conducted at each of these m_1 locations. Therefore, the choice of m_1 needs to balance the size of the region and the computational cost of the preliminary analysis. In our numerical experiments we have maintained m_1 to be in the range of 100 to 500.

The preliminary spotwise analysis provides key information about the variance change point and locationwise estimation accuracy. Denote the data points corresponding to $Z_1 = \{z_j^1, j = 1, \ldots, m_1\}$ by $\{(y_{ij}^1, z_j^1), i = 1, \ldots, N; j = 1, \ldots, m_1\}$. For each fixed location z_j, we apply Gao et al. (2019) to the measurements $\{y_{ij}^1, i = 1, \ldots, N\}$ at the location and obtain the following statistics: change-point estimate $\widehat{\tau}_j^1$ and mean-square error of the mean estimate $\mathrm{MSE}_j^1 = \sum_{i=1}^N \{y_{ij}^1 - \widehat{f}_j^1(i/N)\}^2/N$, where $\widehat{f}_j^1$ the mean-function estimate at location z_j^1. Let $\bar{\tau}^1 = \sum_{j=1}^{m_1} \widehat{\tau}_j^1/m_1$ be the average change-point estimate. These preliminary analysis results will be exploited to guide the next stages of subsampling.

We first use $\bar{\tau}^1$ to narrow down the time range to a window $T = \{t_1, \ldots, t_n\}$ of size n centered at $\bar{\tau}^1$, where $t_1 = \bar{\tau}^1 - \frac{n}{2} + 1, t_2 = \bar{\tau}^1 - \frac{n}{2} + 2, \ldots, t_n = \bar{\tau}^1 + \frac{n}{2}$. The choice of n should balance between the computational cost and the need of sufficient time points for proper

change-point analysis. In our application the variance function of liver surface temperature experiences a sudden drop in magnitude and then sustains the reduced level afterward. For this kind of change point, we generally recommend an n of at least 50 based on our numerical experience. In the paper we use $n = 60$.

The sample size resulted from the first two stages of subsampling is still in the range of thousands or tens of thousands. Therefore, a further reduction of locations is desired. We apply a probability-weighted subsampling approach to Z_1 where the probability weight π_j for each location z_j^1 is calculated as

$$\pi_j = \frac{\sum_{\ell=1}^{m_1}(\mathrm{MSE}_\ell^1 + \varrho_1)}{\mathrm{MSE}_j^1 + \varrho_1} \times \frac{\sum_{\ell=1}^{m_1}(|\widehat{\tau}_\ell^1 - \bar{\tau}^1| + \varrho_2)}{|\widehat{\tau}_j^1 - \bar{\tau}^1| + \varrho_2},$$

where ϱ_1 and ϱ_2 are small positive constants to prevent against zero values. Here, we use $\varrho_1 = 0.0001$ and $\varrho_2 = 0.5$. The motivation for weight π_j is that those locations with "poor" estimates, represented by larger MSE for mean estimate and large deviation of change-point estimate from the average change point, would be less likely to be selected. In our numerical studies we experiment with m values in the range of 10 to 50. Let $Z = \{z_1, \ldots, z_m\}$ be the final subsample of locations. The final subsample of data is now $\{y_{ij} : (t_i, z_j) \in T \times Z, i = 1, \ldots, n, j = 1, \ldots, m\}$ which has a sample size of mn.

2.4. *Iterative estimation on $T \times Z$.* The parameter estimation for the subsample data on $T \times Z$ iterates between: (1) estimate the mean function given estimates of the variance component parameters, and (2) estimate variance component parameters given estimate of the mean function.

For the first step, let the current estimates of variance component parameters be, respectively, $\widetilde{\tau}$, $\widetilde{\sigma}^2(z_j)$ and $\widetilde{\delta}^2(z_j)$, $j = 1, \ldots, m$. In the objective functional (2.2) the response vector $\mathbf{Y}$ becomes $(y_{11}, y_{21}, \ldots, y_{n1}, \ldots, y_{1m}, \ldots, y_{nm})^T$, and the covariance matrix Σ becomes a diagonal matrix whose diagonal repeats $\widetilde{\tau}$ times with the entry $\widetilde{\sigma}^2(z_1)$, $(n - \widetilde{\tau})$ times with the entry $\widetilde{\delta}^2(z_1)$, $\widetilde{\tau}$ times with the entry $\widetilde{\sigma}^2(z_2)$, $(n - \widetilde{\tau})$ times with the entry $\widetilde{\delta}^2(z_2)$ and so on. The mean function f_0 is estimated by the tensor-product splines in Example 2.3 as the minimizer of the penalized weighted least squares (2.2).

Given a mean function estimate $\widetilde{f}$, we extend the testing procedure in Gao et al. (2019) to find an estimate $\widetilde{\tau}$ for the variance change point τ_0. Then, we can compute the maximum likelihood estimates $\widetilde{\sigma}^2(z_j) = \widetilde{\tau}^{-1}\sum_{i=1}^{\widetilde{\tau}}\{y_{ij} - \widetilde{f}(t_i, z_j)\}^2$ and $\widetilde{\delta}^2 = (n - \widetilde{\tau})^{-1}\sum_{i=\widetilde{\tau}+1}^{n}\{y_{ij} - \widetilde{f}(t_i, z_j)\}^2$. For a potential change point position τ, we want to test the hypothesis

$$\begin{aligned} &H_0 : \sigma_{t_1}^2(z) = \cdots = \sigma_{t_n}^2(z) \quad \text{versus} \\ &H_1 : \sigma_{t_1}^2(z) = \cdots = \sigma_{\tau}^2(z) \neq \sigma_{\tau+1}^2(z) = \cdots = \sigma_{t_n}^2(z). \end{aligned} \tag{2.4}$$

Let

$$\ell(\tau) = \sum_{j=1}^{m} \tau \log\left[\frac{1}{\tau}\sum_{i=1}^{\tau}\{y_{ij} - \widetilde{f}(t_i, z_j)\}^2\right] + (n - \tau)\log\left[\frac{1}{n - \tau}\sum_{i=\tau+1}^{n}\{y_{ij} - \widehat{f}(t_i, z_j)\}^2\right].$$

Note that $\ell(n) = -2L_0(\widetilde{\sigma}^2) - mn - mn\log 2\pi$ and $\ell(\tau) = -2L_1(\widetilde{\sigma}^2, \widetilde{\delta}^2) - mn - mn\log 2\pi$, where L_0 and L_1 are, respectively, the log-likelihood functions under the null and alternative hypotheses of (2.4). So we define the test statistic to be $\Delta_n^2 = \max_{1<\tau<n}\{\ell(n) - \ell(\tau)\}$. The asymptotic null distribution for Δ_n^2, together with the convergence rates of all the parameter estimates, are given in Gao et al. (2019).

2.5. *Final estimates*. Although our numerical experiments suggest one subsample can often deliver good estimates with properly chosen m and n, sometimes one may want to repeat the three-stage subsample multiple times with the same parameter values for m_1, m and n. Suppose the subsampling is repeated with replacement K times. Denote the K sets of mean-function and change-point estimates obtained from each subsample as $\{(\widehat{f}_1, \widehat{\tau}_1), \ldots, (\widehat{f}_K, \widehat{\tau}_K)\}$. Then, our final mean and change-point estimates are, respectively, $\widehat{f} = \sum_{k=1}^{K} \widehat{f}_k/K$ and $\widehat{\tau} = \sum_{k=1}^{K} \widehat{\tau}_k/K$.

To get the final estimate of the variance functions, we first use the mean-function estimate $\widehat{f}$ to compute the residuals $\{\hat{\epsilon}_{ij} = y_{ij}^0 - \widehat{f}(i/N, z_j^0), i = 1, \ldots, N; j = 1, \ldots, M\}$. Use thin-plate splines to smooth the squared residuals $\{\hat{\epsilon}_{ij}^2, i = 1, \ldots, \widehat{\tau}; j = 1, \ldots, M\}$ and $\{\hat{\epsilon}_{ij}^2, i = \widehat{\tau} + 1, \ldots, N; j = 1, \ldots, M\}$, respectively, to obtain the final variance function estimates $\widehat{\sigma}^2(z)$ and $\widehat{\delta}^2(z)$.

3. Simulations. In this section we report simulations to evaluate the empirical performance of the proposed method. We considered two different mean functions $f_{01}(t, z) = 20 + 12t(1 - t) + \sin(2\pi z_1) + \cos(2\pi z_2)$ and $f_{02}(t, z) = \sin(t) + t^5 - 8t^3 + 10t + 6 + \sin(2\pi z_1) + \cos(2\pi z_2)$. The first function f_{01} had a surface similar to the estimated mean-temperature function in the procurement study and the second function f_{02} represented a more complex smooth surface. The true variance functions before and after the change point τ_0 were, respectively, $\sigma_0^2(z) = 0.18 + \frac{2}{3}\{(z_1 - 0.5)^2 + (z_2 - 0.5)^2\}$ and $\delta_0^2(z) = 5|\sigma_0^2(z) + (z_1 - 0.5)^3 + (z_2 - 0.5)^3|$, mimicking the variance trends shown in the application. The number of time points was fixed to be $N = 130$, same as the number of time points in the application. The variance function change point was always $\tau_0 = N/2 = 65$. The locations were a 20×20 regular grid on the square domain $[0, 1] \times [0, 1]$ and, thus, $M = 400$. We also fixed the number of blocks in the first stage of location subsampling to be $m_1 = 100$. All the simulations were run on the Windows Server 2012 R2 64 bit with Intel(R) Xeon(R) CPU E5-2650 0 @ 2.00 GHz (two processors) and 64 GB RAM.

3.1. *Computational time comparison*. We first conducted a small scale experiment to compare the computational time of the proposed method for various location subsample sizes with that of the method without any subsampling. One can think of the latter as having $m = M$ and $n = N$. Five data replicates with true mean function f_{01}, $M = 400$ and $N = 130$ were generated. For the method with subsampling, we considered four different subsample sizes of locations, namely, $m = 10, 20, 30$ and 50. For the method without subsampling, all the simulations with $M = 400$ aborted due to memory overflow. Therefore, for a better comparison we reduced M to 100 so that the simulation without subsampling could finish without memory issues. The computational time for each setting was obtained as the average running times on the five replicates. The result is summarized in Table 1. As we can see, even with a much reduced M, the method without subsampling must take more than an hour to finish, compared with the few minutes of the method with subsampling. Since the viability duration of an organ is generally in hours, the subsampling approach is clearly much more appealing here.

TABLE 1
Computational time comparison. NA indicates aborted simulations due to memory overflow

Method	With subsampling				Without subsampling	
n (# time points)	60				130	
m (# locations)	10	20	30	50	100	400
Running time (seconds)	100.97	120.37	132.57	218.54	3921.08	NA

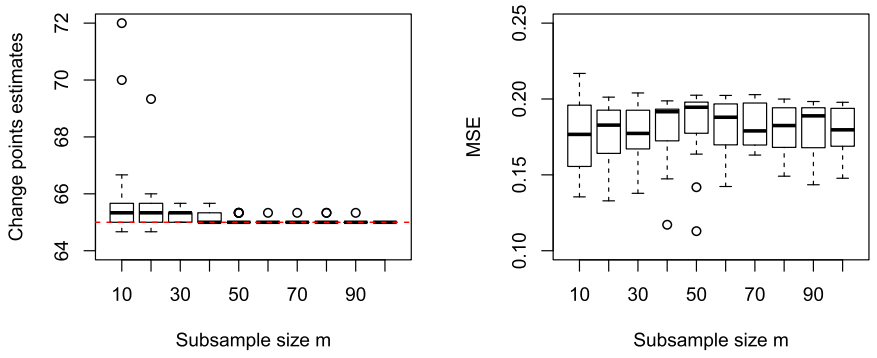

FIG. 2. *Sensitivity analysis for m with* $f_0 = f_{01}, n = 60$ *and* $K = 3$ *for simulations in Section 3.2. Left: Change–point estimates vs. m. Right: MSEs vs. m. The red dashed line represents the true change point* $\tau_0 = 65$.

3.2. *Sensitivity analysis*. The subsampling part has three important tuning parameters, namely, the window size n, the size m of the location subsample and the number K of subsample repetitions. We now present some sensitivity analysis experiments to guide our practical selection of these parameters. Note that m_1, the number of blocks or the initial subsample size of locations, does not appear to be as critical as m based on our numerical experience. So, for brevity, a sensitivity analysis on m_1 is not conducted here. We chose to present the experiments when the true mean function was set to f_{01} which mimics that in our application. We use boxplots of change-point estimates and MSEs to assess the estimation performance, with each boxplot produced from 20 runs under its corresponding simulation setting. Similar analysis can be performed on f_{02} but is skipped here for space concern.

In our first set of experiments, we fixed $n = 60$ and $K = 3$ while letting m taking values from $\{10, 20, \ldots, 100\}$. As shown in Figure 2, the performance, especially the change-point estimation, started to stabilize when $m = 30$. This was also confirmed by our single-run simulations in the Supplementary Material (Gao et al. (2020)) where function estimates with $m = 10$ and $m = 30$ were visually compared. One can surely argue, based on Figure 2, that $m = 50$ can yield even more accurate change-point estimates but that would mean an increase of time cost by approximately $(50/30)^{9/5} - 1 \approx 1.5$ folds. Therefore, we suggest to use $m = 30$ while holding $m = 50$ as a backup option. Our single-run simulations in the Supplementary Material (Gao et al. (2020)) also supports this choice of m.

In the second set of experiments, we fixed $m = 30$ and $K = 3$ while letting n taking values from $\{30, 40, \ldots, 90\}$. In Figure 3, while the MSE boxplots were similar for different n, change-point estimates clearly stabilized to the true value when $n = 60$.

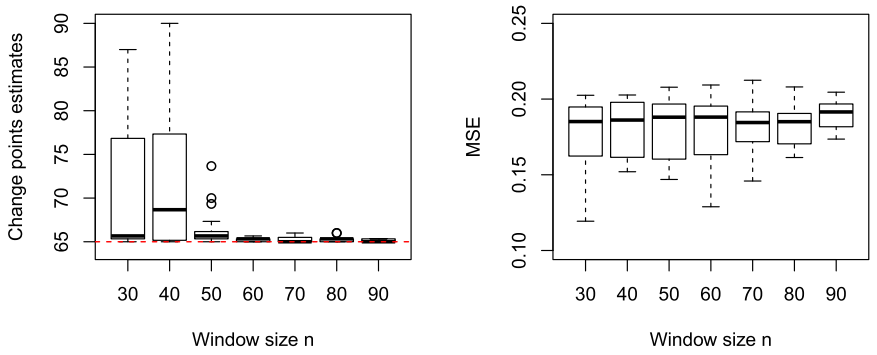

FIG. 3. *Sensitivity analysis for n with* $f_0 = f_{01}, m = 30$ *and* $K = 3$ *for simulations in Section 3.2. Left: Change–point estimates vs. n. Right: MSEs vs. n. The red dashed line represents the true change point* $\tau_0 = 65$.

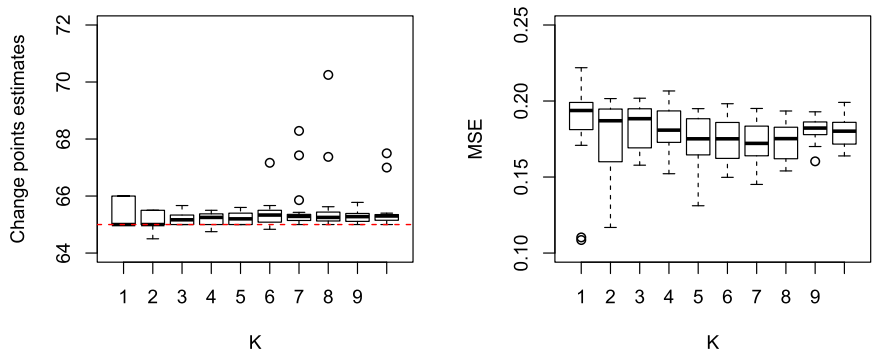

FIG. 4. *Sensitivity analysis for K with $f_0 = f_{01}$, $m = 30$ and $n = 60$ for simulations in Section 3.2. Left: Change-point estimates vs. K. Right: MSEs vs. K. The red dashed line represents the true change point $\tau_0 = 65$.*

In the last set of sensitivity analysis experiments, we fixed $m = 30$ and $n = 60$ while letting K vary from 1 to 10. The boxplots in Figure 4 shows that both the change-point estimates and the MSEs stabilized when at least $K = 3$ repetitions were used.

Based on the above sensitivity analysis, we shall always apply the proposed method with $m = 30$, $n = 60$ and $K = 3$ from now on.

3.3. *Estimation performance.* To assess the estimation performance we repeated the simulations with 1000 data replicates for both true mean functions f_{01} and f_{02}. The boxplots of change-point estimates and MSEs of mean-function estimates are shown in Figure 5. Clearly, the change-point estimates were almost perfect, and the MSEs were well in control in both scenarios. On the other hand, the nearly perfect change-point estimates also indicates that the two variance functions, chosen to mimic the trends in the application, are well separable. Therefore, to demonstrate the robustness of the proposed method, we also considered a scenario where the variance function $\delta_0^2(z)$ was reduced by a factor of 0.56. The resulting boxplots of estimates are in Figure 6. We can see that the estimates were still very accurate. This demonstrates excellent estimation performance of the proposed method.

4. Application: Temperature monitoring in liver procurement. As reviewed in the Introduction, organ viability assessment is a critical step in organ transplant procedures. Unfortunately, the current assessment procedures may suffer from either human subjectivity (visual inspection) or intrusiveness (biopsy). Aiming to find a new, noninvasive way of assessing the viability of organs, a research team from Virginia Tech designed a temperature monitoring system such that the surface temperature of a perfused organ can be densely and continuously monitored using high-resolution infrared thermography (FLIR Systems, Boston, MA). In the experiment considered in this paper, a lobe of porcine liver, as shown in the right panel of Figure 1, was perfused with a physiologic perfusion fluid called modified Krebs' solution (Demmy et al. (1997), Quan et al. (2003), Vargaftig and Hai (1972)). Organ surface temperature was intensively monitored for a continuous period of 24 hours. The liver lobe was optically (not physically) divided into a dense grid of 36,795 spots with each spot producing a 24-hour temperature profile. Temperature measurements were collected every 10 minutes, yielding a total of 145 points in each profile. The first 2.5 hours of data were discarded since it took about one to two hours for the perfusion fluid to completely infuse and stabilize the liver. There were $n = 130$ points left in each profile, after correction and elimination of the data collected during initial infusion and stabilization. In earlier work

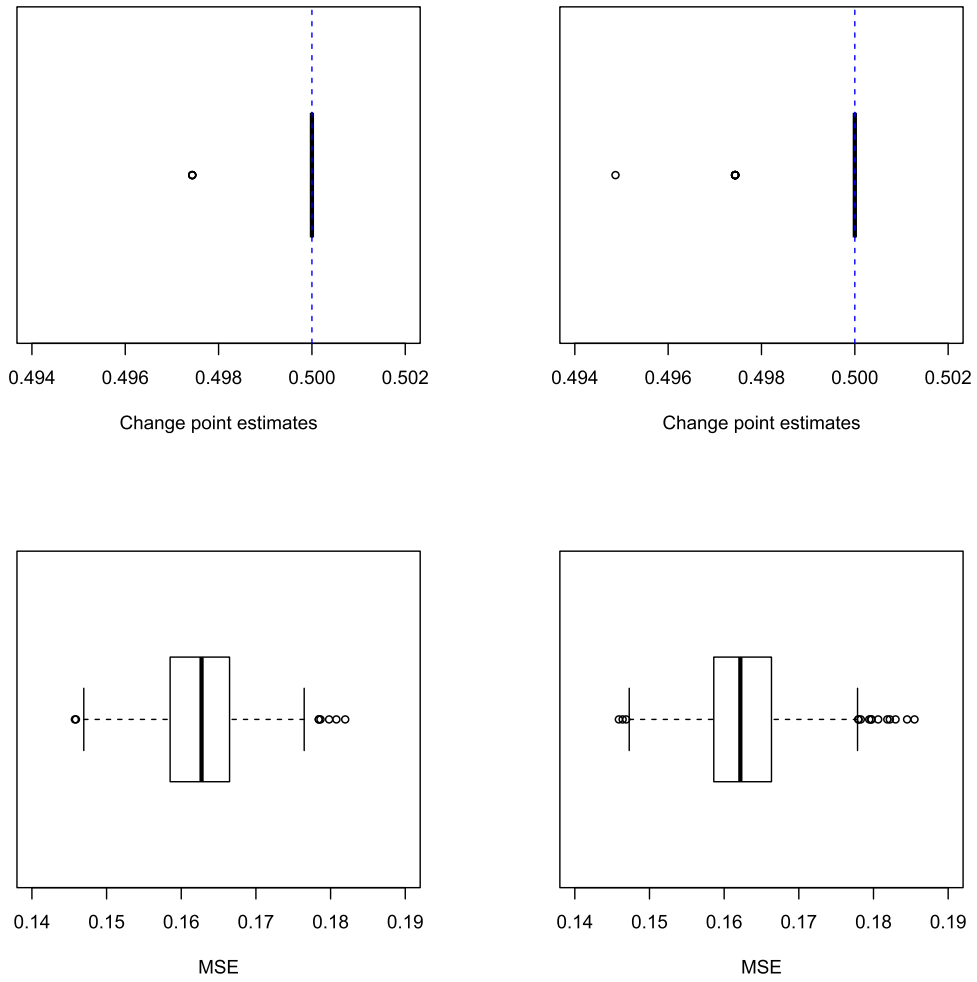

FIG. 5. *Boxplots of change-point estimates* (*top panels*) *and MSEs of mean-function estimates* (*bottom panels*). *Left*: *Simulations with the true mean function* $= f_{01}$; *Right*: *Simulations with the true mean function* $= f_{02}$. *Blue dashed lines represent the true change point* $\tau_0/N = 0.5$.

Gao et al. (2019) conducted a spotwise analysis on each of the 36,795 temperature profiles and produced the heat map of spotwise variance change points shown in Figure 1. We shall now demonstrate how the surfacewise method proposed in this paper can help physicians pinpoint the viability breakdown point in an efficient way for a segment of or the whole liver.

We selected three distinct areas from the liver surface with decreasing levels of uniformity in the spotwise variance change-point estimates, as shown in Figure 7. The numbers of location spots in the areas were, respectively, 6177, 6563 and 6480. We applied the proposed method with $m = 30$, $n = 60$, and $K = 3$ to each of these three pieces of liver. The computational times for the analysis of these areas were, respectively, $44.50s$, $52.01s$ and $38.98s$. The estimated variance change point $\hat{\tau}$ were 12.33 (12.17, 13.17, 11.67), 12.11 (13.00, 12.17, 11.17) and 12.39 (12.17, 11.17, 13.83) hours for areas #1 to #3, respectively, where the numbers in the brackets are the corresponding estimates from the three repetitions. To compare with the results from the spotwise analysis, we plotted the heatmaps and boxplots of variance change point estimates from the spotwise analysis for areas #1 to #3 in Figures 8 to 10.

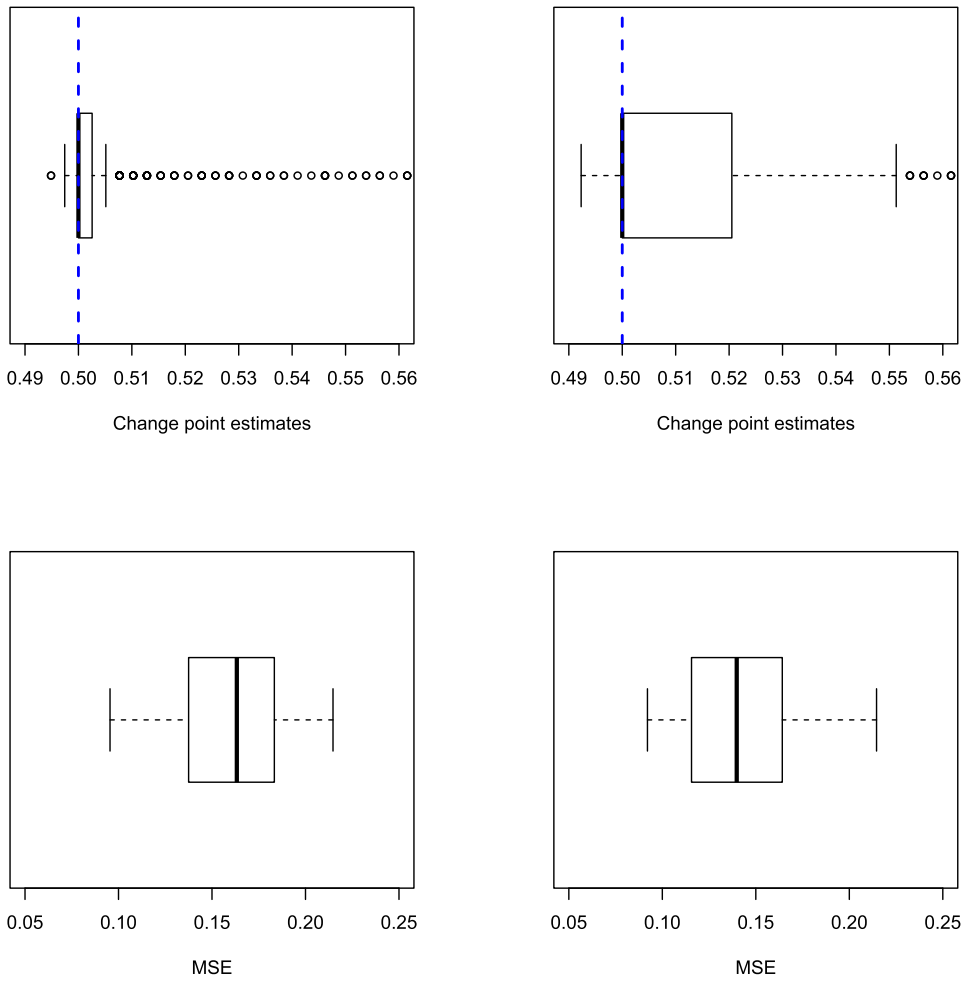

FIG. 6. *Boxplots of change-point estimates* (*top panels*) *and MSEs of mean-function estimates* (*bottom panels*) *with reduced* $\delta_0^2(z)$. *Left*: *Simulations with the true mean function* $= f_{01}$; *Right*: *Simulations with the true mean function* $= f_{02}$. *Blue dashed lines represent the true change point* $\tau_0/N = 0.5$.

Area #1 was a portion of the liver that had the most uniform spotwise change points. It was reassuring to see that the single change-point estimate from our surface-wise method fell right into the middle of the narrow range of the spotwise change points in this area. Area #2 had a wider range of spotwise change points. The single change-point estimate for this area could still fit well into the overall trend of the range. Note that a noticeable portion of spots had their change points beyond 13 hours. But the single change-point estimate could safely tune down the influence of these spots thanks to the three-stage subsampling schemes embedded in the proposed method. Area #3 was much more heterogeneous, with the spotwise change points mostly ranged from 12 to 17 hours. Therefore, it may not be considered appropriate for a surface-wise analysis. It was selected intentionally to see if the proposed surface-wise analysis could return a reasonable change-point estimate for a highly heterogeneous area. Figure 10 shows that the single change point at 13.13 hours is indeed located around the center of all the spotwise change points.

5. Conclusion and discussion. Motivated by the need of monitoring surface temperature in a liver procurement experiment, we have proposed in this paper a variance *func-*

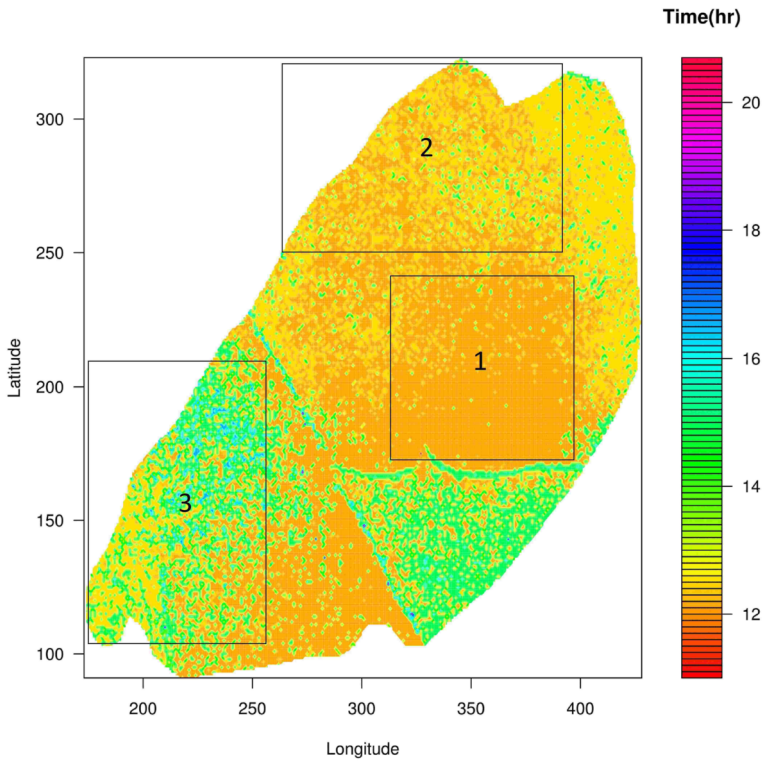

FIG. 7. *The heat map of estimated variance change points of temperatures on the organ surface in the liver procurement experiment with three selected areas. Area* #1: *latitude* [175, 245], *longitude* [312, 398]; *Area* #2: *latitude* [251, 320], *longitude* [261, 394]; *Area* #3: *latitude* [104, 213], *longitude* [175, 255].

tion change-point detection method under a smoothly-changing mean *function* for temperatures measured on a surface and over time. It is a nontrivial multidimensional extension to the recently proposed variance change-point detection method by Gao et al. (2019) under a smoothly-changing mean trend. In addition, such an extension brings significant numerical challenge due to the computational burden of thin-plate splines and its tensor product with cubic splines. We have also developed a three-stage subsampling procedure that can carry out such analysis in a computationally efficient way.

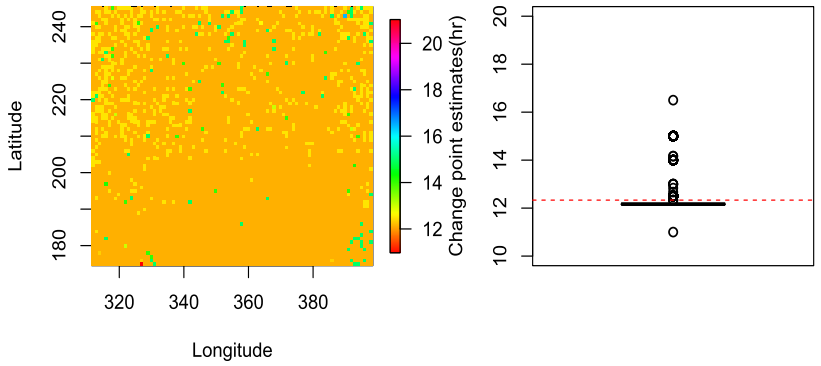

FIG. 8. *Variance change-point estimates for area* #1. *Left*: *heat map of the estimated variance change points from spotwise analysis. Right*: *boxplot of the estimated change points from spotwise analysis for area* #1, *red dashed line is the estimated change point* (12.33 *hours*) *from applying the new method to area* #1.

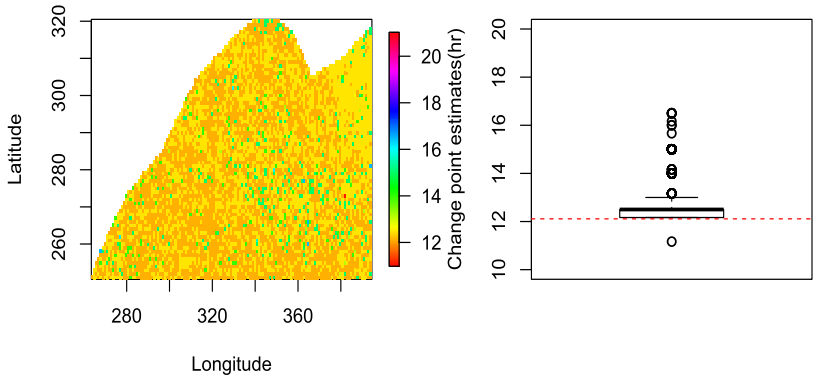

FIG. 9. *Variance change-point estimates for area* #2. *Left*: *heat map of the estimated variance change points from spotwise analysis*. *Right*: *boxplot of the estimated change points from spotwise analysis for area* #2, *red dashed line is the estimated change point* (12.11 *hours*) *from applying the new method to area* #2.

In the proposed method we have assumed independence of observations in space and time. The inclusion of spatial dependence would have difficulty in the specification of an appropriate spatial correlation matrix. The surface temperature of the liver in a region depends on the distribution of blood vessels near the region. Such spatial variation can be hardly represented by common spatial correlation matrices. For the time domain dependence, our exploration shows that the observations might have short-memory dependence. As well known for nonparametric smoothing, ignorance of such dependence won't affect the consistency of a nonparametric smooth mean function estimate; see, for example, Lin and Carroll (2001). On the other hand, its potential influence on variance estimation can become very complicated. Work in these dependence-incorporated directions surely merit more research and is ongoing within the research team.

Another common approach to reducing sample size is data aggregation which may have some difficulty in our application. First, data aggregation over the spatial domain may obscure the underlying change point pattern due to the spatial heterogeneity of variance over the surface. This can complicate the subsequent change-point analysis. Second, once the data are aggregated, it is hard to run any spotwise analysis, whereas spotwise analysis provides useful information and plays a critical role in our multistage subsampling approach.

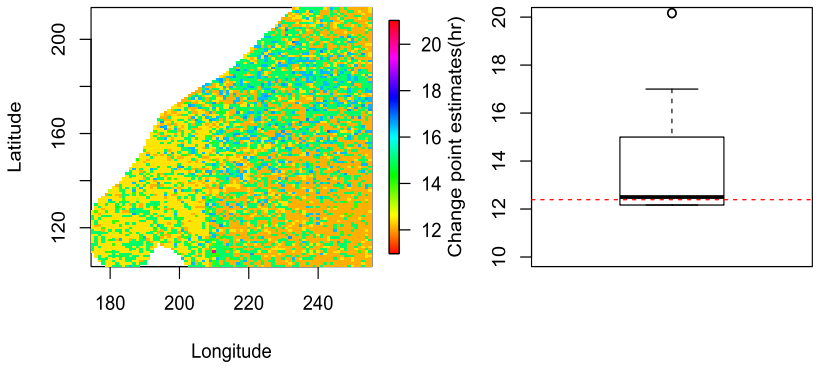

FIG. 10. *Variance change-point estimates for area* #3. *Left*: *heat map of the estimated variance change points from spotwise analysis*. *Right*: *boxplot of the estimated change points from spotwise analysis for area* #3, *red dashed line is the estimated change point* (12.39 *hours*) *from applying the new method to area* #3.

Acknowledgments. Du's research was supported by NSF Grants DMS-1620945 and DMS-1916174. Part of the data collection and experimental efforts was supported by NSF Grant CMMI-1435996. The authors thank Mr. Qing Lan from the Grado Department of Industrial and Systems Engineering at Virginia Tech for data preprocessing and the editors and reviewers for their insightful comments that have significantly improved the paper.

SUPPLEMENTARY MATERIAL

Supplement to "Surface temperature monitoring in liver procurement via functional variance change point analysis" (DOI: 10.1214/19-AOAS1297SUPP; .pdf). We conducted single-run simulations to study the choice of the location subsample size m.

REFERENCES

BERKES, I., GABRYS, R., HORVÁTH, L. and KOKOSZKA, P. (2009). Detecting changes in the mean of functional observations. *J. R. Stat. Soc. Ser. B. Stat. Methodol.* **71** 927–946. MR2750251 https://doi.org/10.1111/j.1467-9868.2009.00713.x

BHONSLE, S., BONAKDAR, M., NEAL II, R. E., AARDEMA, C., ROBERTSON, J. L., HOWARTH, J., KAVNOUDIAS, H., THOMSON, K. R., GOLDBERG, S. N. et al. (2016). Characterization of irreversible electroporation ablation with a validated perfused organ model. *J. Vasc. Interv. Radiol.* **27** 1913–1922.

DEMMY, T. L., BIDDLE, J. S., BENNETT, L. E., WALLS, J. T., SCHMALTZ, R. A. and CURTIS, J. J. (1997). Organ preservation solutions in heart transplantation-patterns of usage and related survival. *Transplant.* **63** 262–269.

DRINEAS, P., MAHONEY, M. W., MUTHUKRISHNAN, S. and SARLÓS, T. (2011). Faster least squares approximation. *Numer. Math.* **117** 219–249. MR2754850 https://doi.org/10.1007/s00211-010-0331-6

DUCHON, J. (1977). Splines minimizing rotation-invariant semi-norms in Sobolev spaces. In *Constructive Theory of Functions of Several Variables* (*Proc. Conf., Math. Res. Inst., Oberwolfach*, 1976) *Lecture Notes in Math.* **571** 85–100. Springer, Berlin. MR0493110

FAN, J., ZHANG, C. and ZHANG, J. (2001). Generalized likelihood ratio statistics and Wilks phenomenon. *Ann. Statist.* **29** 153–193. MR1833962 https://doi.org/10.1214/aos/996986505

FEBRERO, M., GALEANO, P. and GONZÁLEZ-MANTEIGA, W. (2008). Outlier detection in functional data by depth measures, with application to identify abnormal NO_x levels. *Environmetrics* **19** 331–345. MR2440036 https://doi.org/10.1002/env.878

FITHIAN, W. and HASTIE, T. (2014). Local case-control sampling: Efficient subsampling in imbalanced data sets. *Ann. Statist.* **42** 1693–1724. MR3257627 https://doi.org/10.1214/14-AOS1220

GAO, Z., SHANG, Z., DU, P. and ROBERTSON, J. L. (2019). Variance change point detection under a smoothly-changing mean trend with application to liver procurement. *J. Amer. Statist. Assoc.* **114** 773–781. MR3963179 https://doi.org/10.1080/01621459.2018.1442341

GAO, Z., DU, P., JIN, R. and ROBERTSON, J. L. (2020). Supplement to "Surface temperature monitoring in liver procurement via functional variance change-point analysis." https://doi.org/10.1214/19-AOAS1297SUPP.

GU, C. (2013). *Smoothing Spline ANOVA Models*, 2nd ed. *Springer Series in Statistics* **297**. Springer, New York. MR3025869 https://doi.org/10.1007/978-1-4614-5369-7

JIN, R., CHANG, C. J. and SHI, J. (2011). Sequential measurement strategy for wafer geometric profile estimation. *IIE Trans.* **44** 1–12.

KARPELOWSKY, J. S. J. (2014). Near-infrared spectroscopy for monitoring renal transplant perfusion. *Pediatric Nephrology* **29** 2241–2242.

KEEFFE, E. B. (2001). Liver transplantation: Current status and novel approaches to liver replacement. *Gastroenterol.* **120** 749–762.

KIM, Y.-J. and GU, C. (2004). Smoothing spline Gaussian regression: More scalable computation via efficient approximation. *J. R. Stat. Soc. Ser. B. Stat. Methodol.* **66** 337–356. MR2062380 https://doi.org/10.1046/j.1369-7412.2003.05316.x

KOCHAN, K., MASLAK, E., CHLOPICKI, S. and BARANSKA, M. (2015). FT-IR imaging for quantitative determination of liver fat content in non-alcoholic fatty liver. *Analyst* **140** 4997–5002.

LAN, Q., JIN, R. and ROBERTSON, J. L. (2015). Quantitative and qualitative evaluation for organ preservation in transplant. In *IIE Annual Conference, Proceedings* 2229–2236.

LAN, Q., SUN, H., ROBERTSON, J., DENG, X. and JIN, R. (2018). Non-invasive assessment of liver quality in transplantation based on thermal imaging analysis. *Comput. Methods Programs Biomed.* **164** 31–47.

LIN, X. and CARROLL, R. J. (2001). Semiparametric regression for clustered data using generalized estimating equations. *J. Amer. Statist. Assoc.* **96** 1045–1056. MR1947252 https://doi.org/10.1198/016214501753208708

MA, P., MAHONEY, M. W. and YU, B. (2015). A statistical perspective on algorithmic leveraging. *J. Mach. Learn. Res.* **16** 861–911. MR3361306

MA, P. and SUN, X. (2015). Leveraging for big data regression. *Wiley Interdiscip. Rev.: Comput. Stat.* **7** 70–76. MR3348722 https://doi.org/10.1002/wics.1324

O'BRIEN, T. J., ROGHANIZAD, A. R., JONES, P. A., AARDEMA, C. H., ROBERTSON, J. L. and DILLER, T. E. (2017). The development of a thin-filmed noninvasive tissue perfusion sensor to quantify capillary pressure occlusion of explanted organs. *IEEE Trans. Biomed. Eng.* **64** 1631–1637.

QIU, P., ZOU, C. and WANG, Z. (2010). Nonparametric profile monitoring by mixed effects modeling. *Technometrics* **52** 265–277. MR2723706 https://doi.org/10.1198/TECH.2010.08188

QUAN, A., LEUNG, S. W., LAO, T. T. and MAN, R. Y. (2003). 5-hydroxytryptamine and thromboxane A2 as physiologic mediators of human umbilical artery closure. *J. Soc. Gynecol. Investig.* **10** 490–495.

ROKHLIN, V. and TYGERT, M. (2008). A fast randomized algorithm for overdetermined linear least-squares regression. *Proc. Natl. Acad. Sci. USA* **105** 13212–13217. MR2443725 https://doi.org/10.1073/pnas.0804869105

ROTHUIZEN, J. and TWEDT, D. C. (2009). Liver biopsy techniques. *Vet. Clin. North Am., Small Anim. Pract.* **39** 469–480.

SHANG, Z. and CHENG, G. (2017). Computational limits of a distributed algorithm for smoothing spline. *J. Mach. Learn. Res.* **18** Paper No. 108, 37. MR3725447

VARGAFTIG, B. B. and HAI, N. D. (1972). Selective inhibition by mepacrine of the release of "rabbit aorta contracting substance" evoked by the administration of bradykinin. *J. Pharm. Pharmacol.* **24** 159–161.

VAZQUEZ-MARTUL, E. and PAPADIMITRIOU, J. C. (2004). Importance of biopsy evaluation and the role of the pathologist in solid organ transplant programs. *Transplant. Proc.* **36** 725–728.

VIDAL, E., AMIGONI, A., BRUGNOLARO, V., GHIRARDO, G., GAMBA, P., PETTENAZZO, A., ZANON, G. F., COSMA, C., PLEBANI, M. et al. (2014). Nearinfrared spectroscopy as continuous real-time monitoring for kidney graft perfusion. *Pediatric Nephrology* **29** 909–914.

WAHBA, G. (1990). *Spline Models for Observational Data. CBMS-NSF Regional Conference Series in Applied Mathematics* **59**. SIAM, Philadelphia, PA. MR1045442 https://doi.org/10.1137/1.9781611970128

WANG, H., YANG, M. and STUFKEN, J. (2019). Information-based optimal subdata selection for big data linear regression. *J. Amer. Statist. Assoc.* **114** 393–405. MR3941263 https://doi.org/10.1080/01621459.2017.1408468

WANG, H., ZHU, R. and MA, P. (2018). Optimal subsampling for large sample logistic regression. *J. Amer. Statist. Assoc.* **113** 829–844. MR3832230 https://doi.org/10.1080/01621459.2017.1292914

WOODALL, W. H., SPITZNER, D. J., MONTGOMERY, D. C. and GUPTA, S. (2004). Using control charts to monitor process and product profiles. *J. Qual. Technol.* **36** 309–320.

XU, D. and WANG, Y. (2018). Divide and recombine approaches for fitting smoothing spline models with large datasets. *J. Comput. Graph. Statist.* **27** 677–683. MR3863768 https://doi.org/10.1080/10618600.2017.1402775

YU, G., ZOU, C. and WANG, Z. (2012). Outlier detection in functional observations with applications to profile monitoring. *Technometrics* **54** 308–318. MR2967980 https://doi.org/10.1080/00401706.2012.694781

ZHANG, Y., DUCHI, J. and WAINWRIGHT, M. (2015). Divide and conquer kernel ridge regression: A distributed algorithm with minimax optimal rates. *J. Mach. Learn. Res.* **16** 3299–3340. MR3450540

ZOU, C., TSUNG, F. and WANG, Z. (2008). Monitoring profiles based on nonparametric regression methods. *Technometrics* **50** 512–526. MR2477862 https://doi.org/10.1198/004017008000000433